Supplemental Information

Distinct Inhibitory Circuits Orchestrate *beta* and *gamma* Band Oscillations

Guang Chen[1,2], Yuan Zhang[1], Xiang Li[1], Xiaochen Zhao[1], Qian Ye[1], Yingxi Lin[3], Huizhong W. Tao[4],

Malte J. Rasch[1,*] and Xiaohui Zhang[1, 5,*]

Inventory of Supplemental Information

1. Supplemental Figures:

A SOM-Cre × Arch-eGFP (Ai35) | SOM antibody | Merge

B SOM-Cre × ChR2-tdTomato (Ai27) SOM antibody | Merge

C SOM-Cre × ChR2-YFP (Ai32) | SOM (blue) merge | PV (red) merge

D PV-Cre × Arch-eGFP (Ai35) | PV antibody | Merge

E PV-Cre × ChR2-tdTomato (Ai27) PV antibody | Merge

F PV-Cre × ChR2-YFP (Ai32) | SOM (blue) merge | PV (red) merge

G spontaneous, light evoked, r = 0.98

H NS, WS, tagged SOM, tagged PV

I

J

K

L

M SOM-Arch | PV-Arch | SOM-ChR2 | PV-ChR2

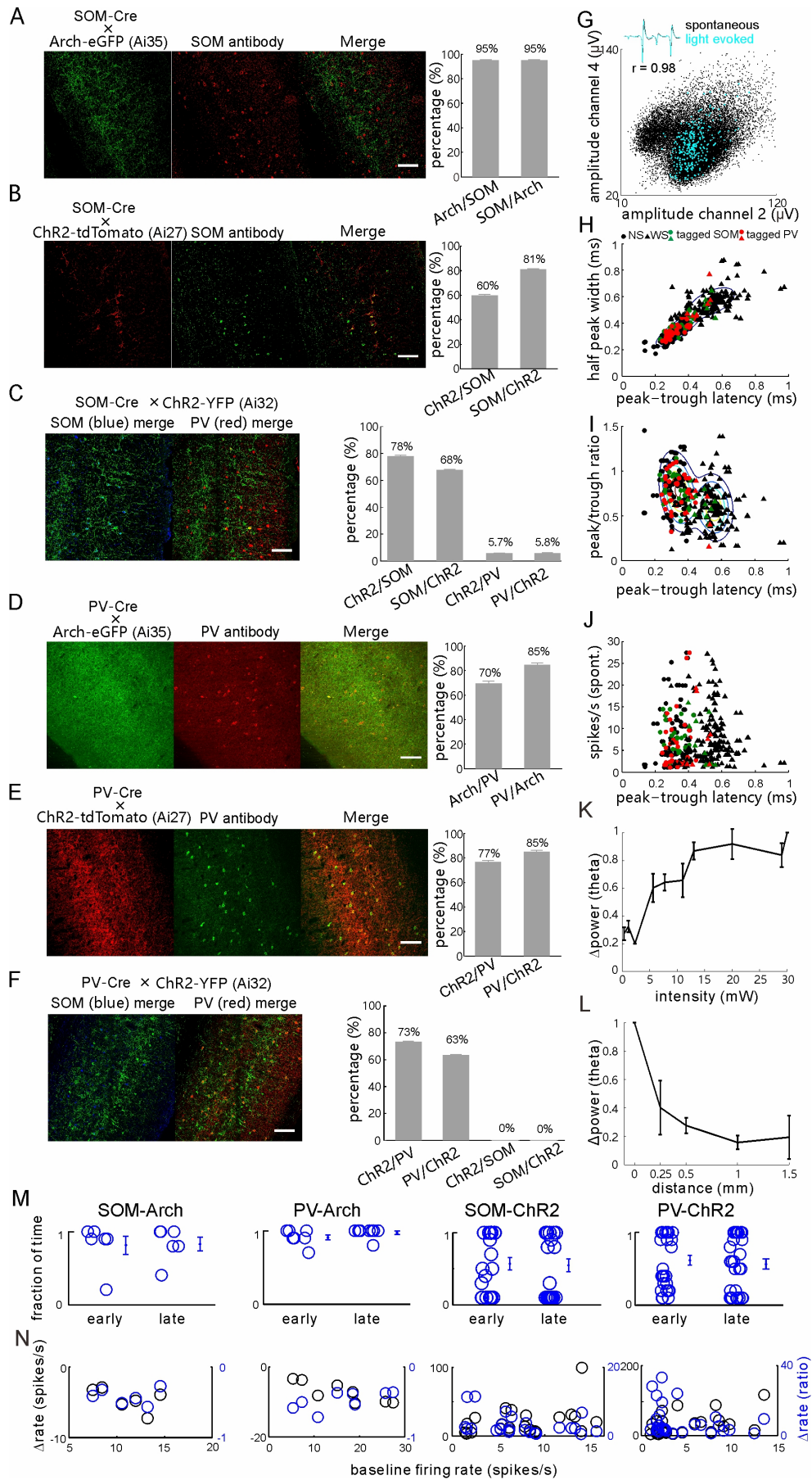**N** baseline firing rate (spikes/s)

Figure S1 related to Figure 1 and Figure 5. Immunostaining and electrophysiological characterization of optogenetic protein-expressing cells in transgenic mice. (A) Left: representative fluorescence images of endogenous GFP (green), immunostaining of antibody against somatostatin (SOM) proteins (red) in the V1 section of *SOM::Ai35* (Arch) mouse. Scale bar, 100 μm. Right: percentages of SOM positive cells that expressed Arch-GFP (efficiency) and of Arch-GFP positive cells that expressed SOM proteins (specificity, n = 12 sections from 3 *SOM::Ai35* mice). (B) Similar to A except for the *SOM::Ai27* (ChR2-tdTomato) mouse (n = 18 sections from 4 mice). (C) Similar to B except for the *SOM::Ai32* (ChR2-EYFP) mouse (n = 18 sections from 4 mice). Note that there is a leakage < 6% to cortical PV cells. (D-F) Similar to A-C except that all immune-characterizations were done in the *PV::Ai35* (Arch, n = 7 sections in 4 mice), *PV::Ai27* (ChR2-tdTomato, n = 7 sections in 3 mice) and *PV::Ai32* (ChR2-EYFP, n = 16 sections in 4 mice) lines, respectively. (G) Example spike sorting and optogenetic tagging. Raw spike waveforms before clustering were plotted in amplitude space from two tetrode channels (channel 2 and 4). Black dots were spontaneous spikes and cyan dots were laser light-evoked spikes. Insert: waveforms of the averaged spontaneous and light-evoked spikes, showing high shape correlation (r = 0.98). (H) A plot of the peak-trough latency *vs* the half peak width of spike waveforms to classify the wide-spiking (WS) and narrow-spiking (NS) cells, including 29 optogentic tagged cortical SOM cells (green) and 38 PV cells (red). Individual dots were jittered (s.d., 8 μs). 2-D Gaussian mixture model (GMM) was fitted with two mixture components to classify the units into two clusters. Ellipses indicate the iso-probability regions for each Gaussian. Circles (NS) and triangles (WS) show the maximum a-posteriori (MAP) classification. (I) A plot of the peak-trough latency *vs* peak/trough ratio of spike waveforms, and others are similar to H. (J) A plot of spontaneous firing rates of the classified and tagged units *vs* their spike waveforms' peak-trough latencies. (K) Induced mean relative changes of LFP theta power (Δpower, normalized to the value at laser intensity of 30 mW) along with increasing laser intensity (n = 35 recording sites, 31 mice). (L) Induced mean relative changes of LFP theta power (normalized to the value at distance of 0 mm) along with increasing spatial distance (horizontal) between the optic fiber and the recording electrode (n = 4 recording in 4 mice). Error bars represent s.e.m. (M) Fraction of time during which laser light evoked significant firing rate changes (*vs* baseline rate) on tagged cells in the early and late half of the whole stimulation period for SOM-Arch, PV-Arch, SOM-ChR2 and PV-ChR2 mice, respectively. (N) Laser light-evoked absolute (black) and relative (blue) firing rate changes (*vs* baseline rate) on tagged cells for SOM-Arch, PV-Arch, SOM-ChR2 and PV-ChR2 mice, respectively.
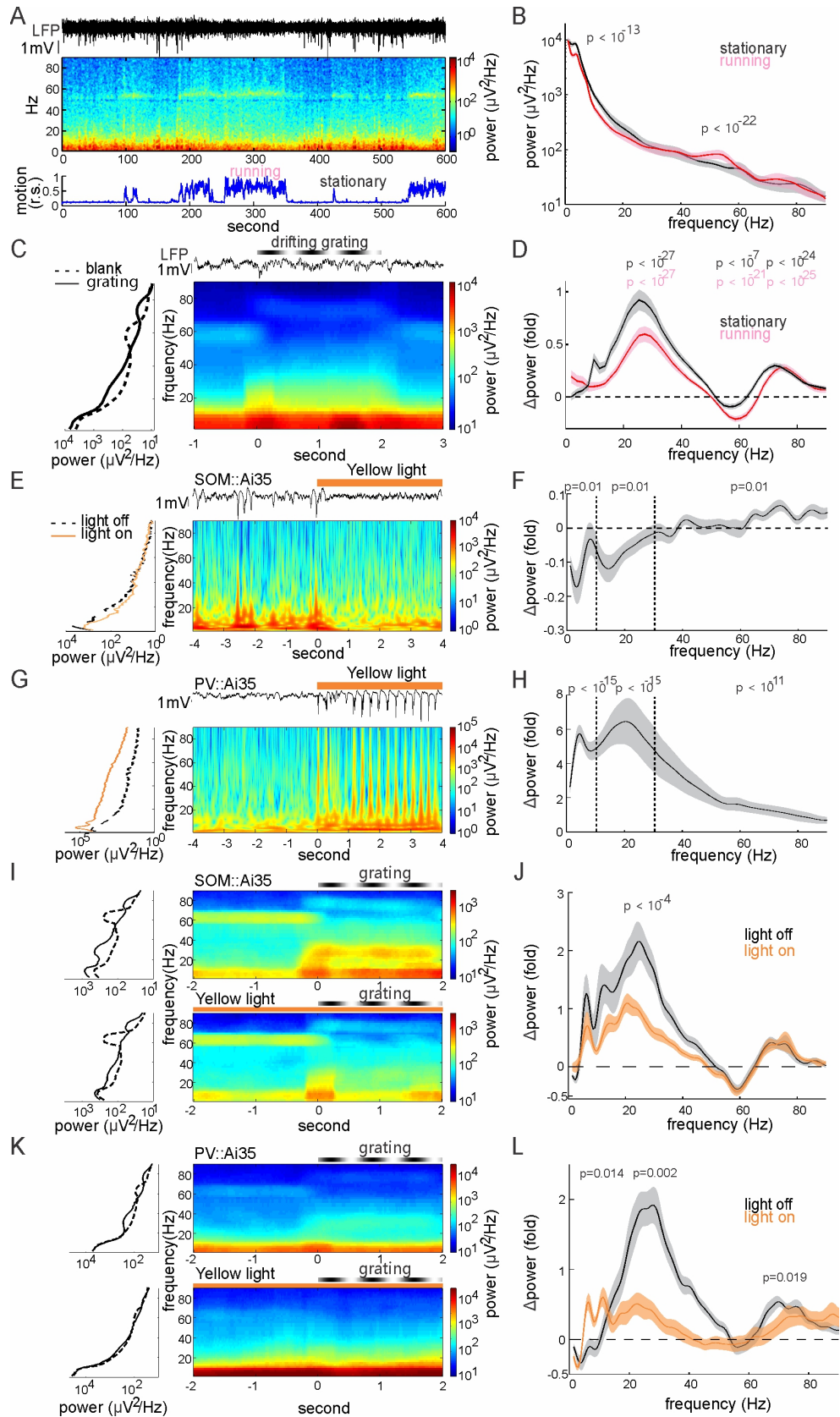
Figure S2 related to Figure2, Figure 3, Figure 5 and Figure 6. LFP power spectra calculated without pre-whitening processing. (A) Example local field potential (LFP) raw trace (top), corresponding power spectrogram (middle) and the animal motion trace (relative speed, r.s., bottom). (B) Mean LFP power spectrum of all recording during the stationary and running states. Shaded areas indicate s.e.m. (n = 274 recording in 61 mice, 1-20 Hz: $p < 10^{-13}$, 40-70 Hz: $p < 10^{-22}$, Wilcoxon two-sided signed rank test). (C) Examples of raw LFP trace (top), trial averaged peri-stimulus spectrogram (bottom right) and the averaged power spectrum (over time) along frequency before and during drifting grating stimulation (bottom left). (D) Mean LFP power changes (power: [grating-blank]/blank) induced by grating stimulation during stationary (black) and running (red) states (shaded area indicates s.e.m., n = 131 recording sites in 44 mice, p values of power changes around (±5 Hz) peak frequencies in three bands: 15-40, 55-65 and 65-80 Hz were calculated by Wilcoxon two-sided signed rank test). (E) Examples of LFP trace and the corresponding time-frequency spectrogram aligned to the onset (at 0 s) of 4 s yellow light (589nm, 30 mW) in the V1 of *SOM::Ai35* mouse. left insert: averaged power spectrum (over time) along frequency during the light OFF (black line) and ON (yellow) conditions. (F) Mean changes of LFP power over frequency induced by yellow light stimulation (data from stationary and running states was pooled together. 5-30 mW, Δpower = [power$_{light\,on}$ − power$_{light\,off}$]/power$_{light\,off}$, n = 21 recording sites in 7 mice; p values for 1-10 Hz, 10-30 Hz, 40-80 Hz were computed by Wilcoxon two-sided signed rank test). (G and H) Similar to E and F but for *PV::Ai35* mice (n=119 recording sites in 30 mice). (I) Trial averaged LFP time-frequency spectrogram (right) and the plot of averaged power spectra over time during the blank (2 s duration) and 2-s drifting grating stimulation periods (left) in the absence (top) or presence (bottom) of 6-s yellow light stimulation in V1 of a *SOM::Ai35* mouse (bottom). (J) Comparison of the visually induced mean change of LFP power spectral (Δpower = [power$_{grating}$ − power$_{blank}$]/power$_{blank}$, top) between the periods of light ON (yellow) and OFF (black). The p values for power in each frequency bands (mean power in 1-10 Hz, mean power around peak frequencies in 15-40 Hz, 55-65 Hz and 65-80 Hz) were calculated by Wilcoxon two-sided signed rank test (n=16 recording in 8 mice, light OFF vs light ON). (K and L) Similar to I and J but for *PV::Ai35* mice (n = 12 recording in 10 mice). All shaded areas represent the s.e.m.
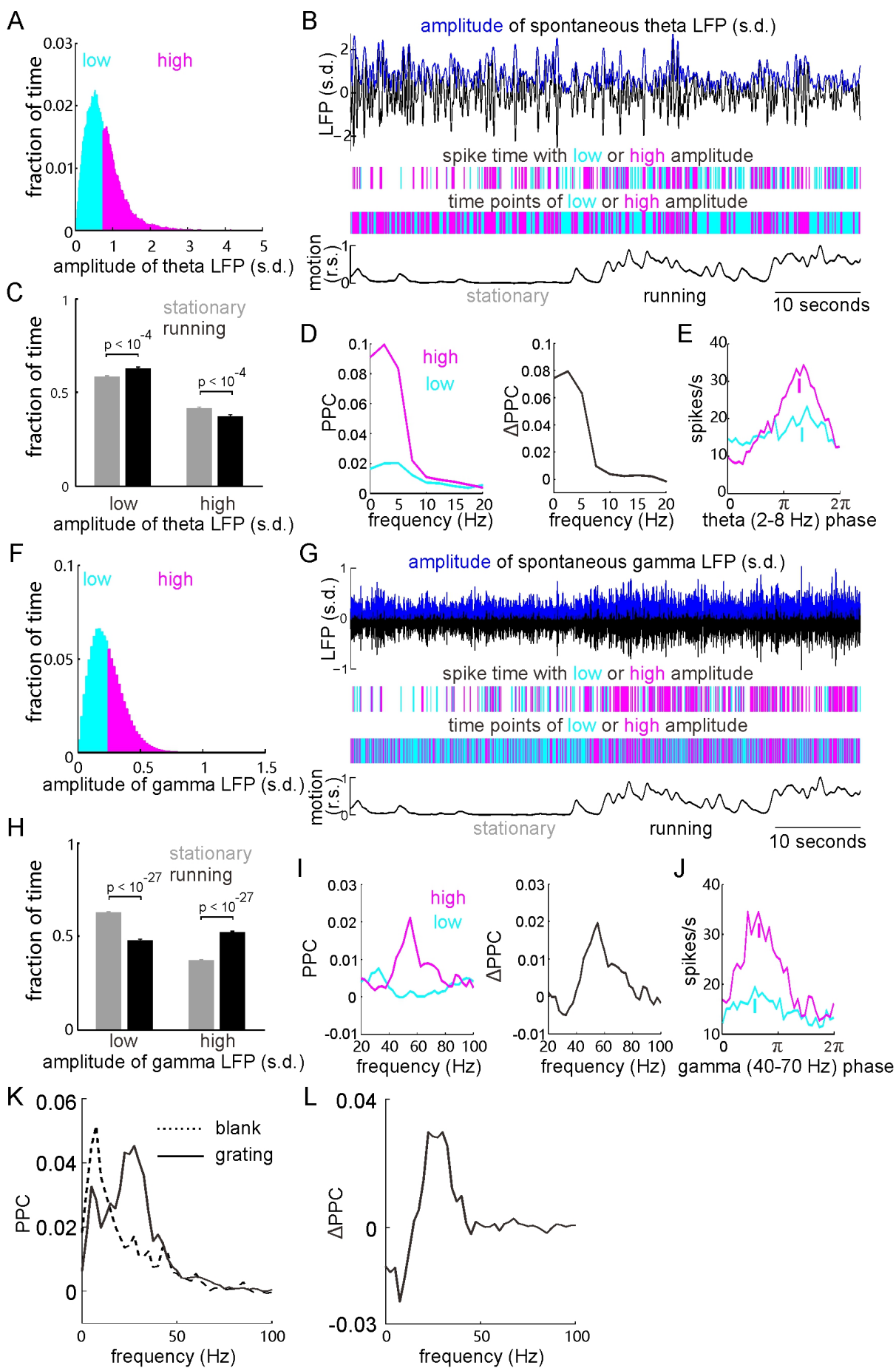
Figure S3 related to Figure 2 and Figure 3. Illustration of spontaneous LFP amplitude triggered PPC change, visually induced PPC change and phase locking of spikes. (A) Distribution of LFP theta (2-8 Hz) amplitude (measured as its standard deviation, s.d.) over time in an example recording. The amplitude at each time point was classified into low (cyan) or high (pink) by the total mean amplitude. (B) Theta band LFP trace (black) and the corresponding amplitude envelope (blue) calculated by Hillbert transformation (top). Time points of the LFP trace and the spiking time of an example unit accompanied with low or high theta amplitude were indicated by cyan or pink lines, respectively (middle). The relative motion (moving speed, r.s.) of the animal was shown in black line (bottom). The behavior states were classified into stationary and running by the global mean value of r.s. (C) Time fraction of low and high LFP theta amplitudes during the stationary and running states in a whole recording were compared (n =165 recording sites, 61 mice; *Wilcoxon* two-sided signed rank test). Error bars represent s.e.m. (D) Left: spike-LFP pairwise phase consistency (PPC) of an example unit calculated from spikes fired at time points of low and high theta amplitudes was shown by the cyan (PPC_{low}) and pink (PPC_{high}) lines, respectively. Right: the LFP theta amplitude triggered change of PPC ($\Delta PPC = PPC_{high} - PPC_{low}$). (E) Distributions of transient firing rate over the LFP theta phase for spikes fired at time points of low and high theta amplitudes were shown in cyan and pink lines, respectively. Short bars indicate the preferred phases. (F-J) Similar to A-E except for analyses of the LFP gamma (40-70 Hz) amplitude, gamma amplitude triggered PPC change and the phase locking of spikes. (K) PPC of an example unit during the baseline (blank) and the grating stimulation periods. (L) Grating-induced change of PPC ($\Delta PPC = PPC_{grating} - PPC_{blank}$).
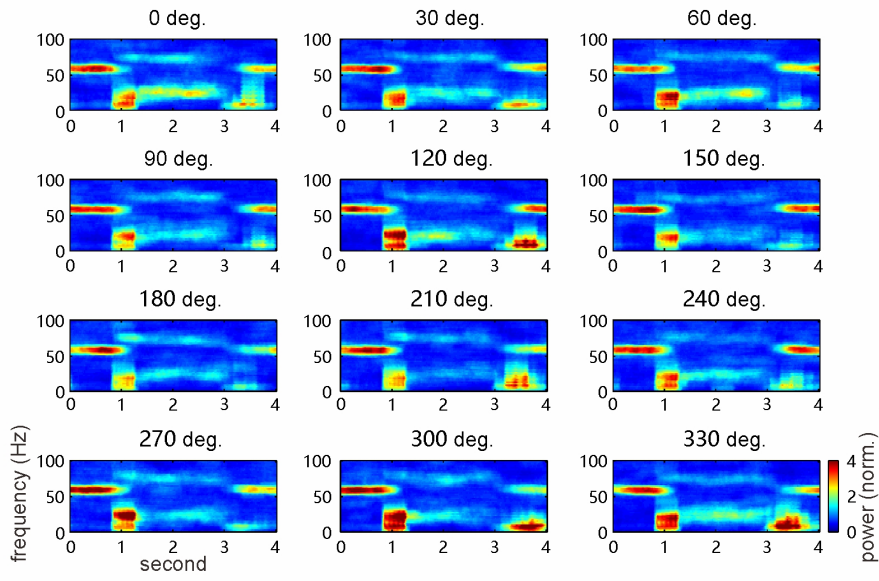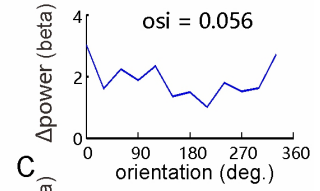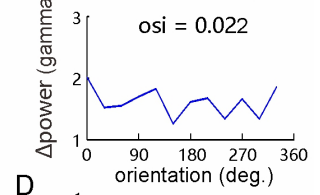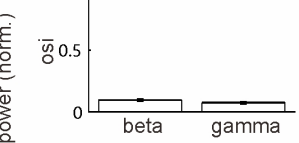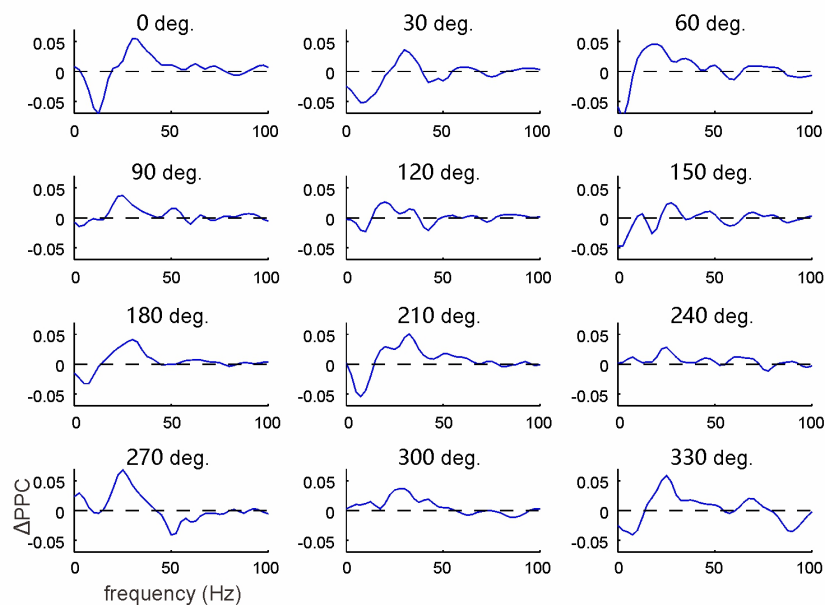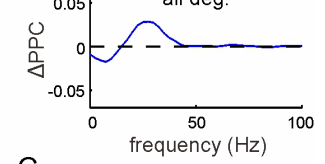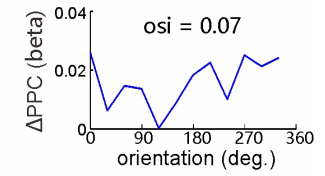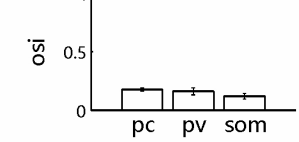
Figure S4 related to Figure 3. Weak orientation tuning of visually induced oscillations. (A) Examples of trial averaged peri-stimulus LFP spectrograms induced by drifting gratings with 12 different directions. (B) Visually induced beta band (around peak frequencies in 15-40 Hz) power changes (Δpower = [power$_{grating}$ − power$_{blank}$]/power$_{blank}$) over the orientations. Top: orientation selective index (osi) for visually induced power change. (C) Visually induced gamma band (around peak frequencies in 65-80 Hz) power changes over the orientations. (D) Summary of the osi for visually induced beta and gamma band power changes of all recording (n = 64 recording sites, 29 mice). (E) Examples of trial averaged visually induced PPC changes (ΔPPC = PPC$_{grating}$ − PPC$_{blank}$) by drifting gratings with 12 different directions. (F) Averaged visually induced PPC change over 12 directions. (G) Changes of visually induced beta band PPC over the 12 directions. Top: the osi value. (H) The population average osi of induced beta band PPC changes for recorded PCs (n = 74 units), tagged PV cells (n = 30) and tagged SOM cells (n = 12), respectively. Error bars represent s.e.m.
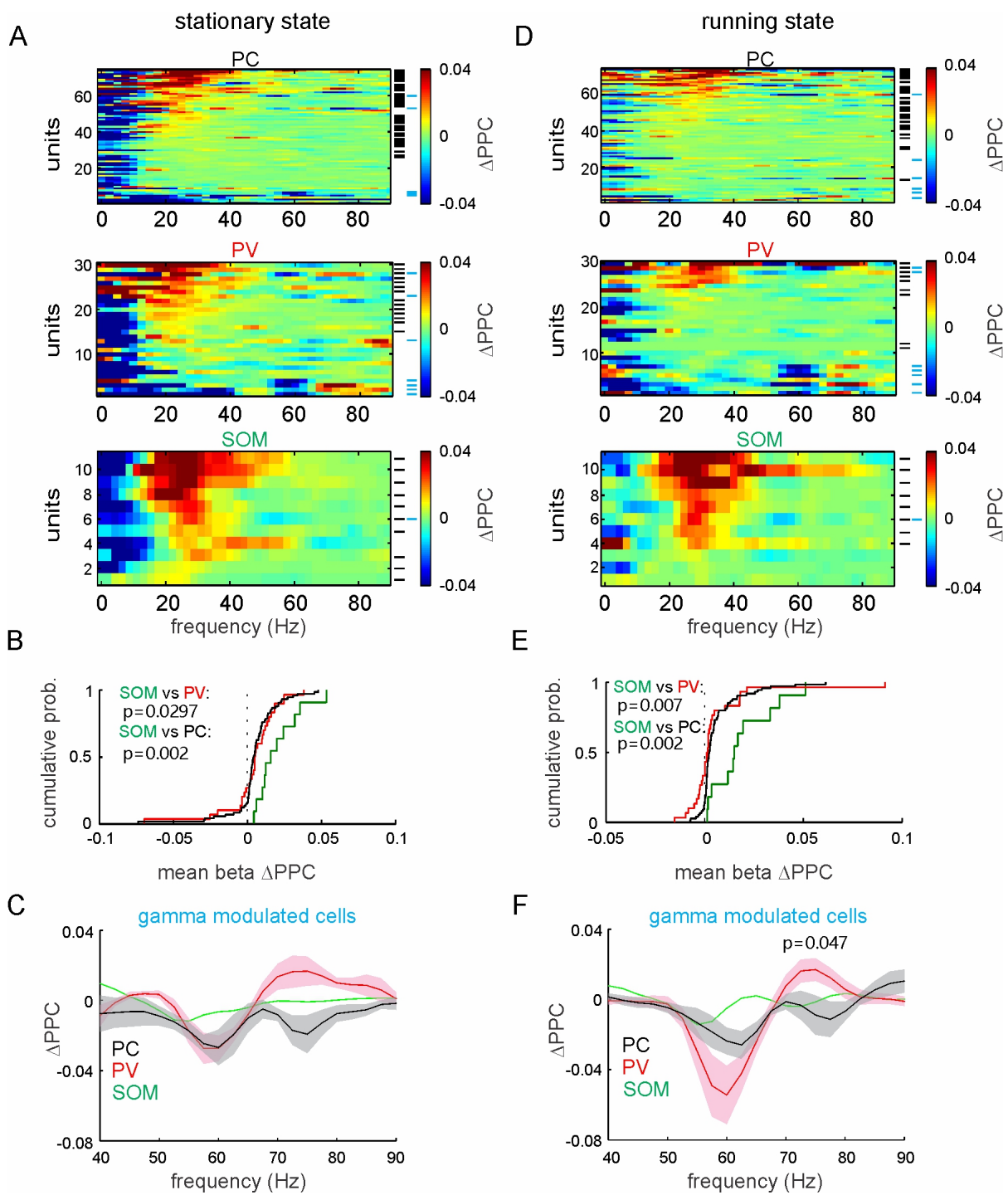
A stationary state

PC

PV

SOM

frequency (Hz)

B

cumulative prob.

SOM vs PV:
p=0.0297
SOM vs PC:
p=0.002

mean beta ΔPPC

C gamma modulated cells

ΔPPC

PC
PV
SOM

frequency (Hz)

D running state

PC

PV

SOM

frequency (Hz)

E

cumulative prob.

SOM vs PV:
p=0.007
SOM vs PC:
p=0.002

mean beta ΔPPC

F gamma modulated cells

p=0.047

ΔPPC

PC
PV
SOM

frequency (Hz)

Figure S5 related to Figure 3. Visually induced PPC changes during stationary and running states. (A) Visually induced PPC changes (ΔPPC = PPC$_{grating}$ − PPC$_{blank}$) in the PCs (n = 74, top), tagged PV cells (n = 30, middle) and tagged SOM cells (n = 11, bottom) during stationary state. Units were ranked by values of mean ΔPPC in beta band (peak frequency $\pm$5 Hz in 15-40 Hz range), and those units showing significant increase of induced beta-band PPC or changes of gamma-band PPC (decrease in 50-65 Hz gamma band or increase in 65-80 Hz high gamma band) are labeled by short black bars (beta modulated cells) or cyan bars (gamma modulated cells, $p < 0.01$, permutation test), respectively. (B) Cumulative distributions of beta band ΔPPC of the PCs, tagged SOM and PV cells. The p values were computed by *Kolmogorov-Smirnov* test. (C) Plots of ΔPPC (40-90 Hz range) of gamma modulated cells as indicated in A by cyan bars. (D-F) Similar to A-C but for data from running state. All shaded areas represent the s.e.m.
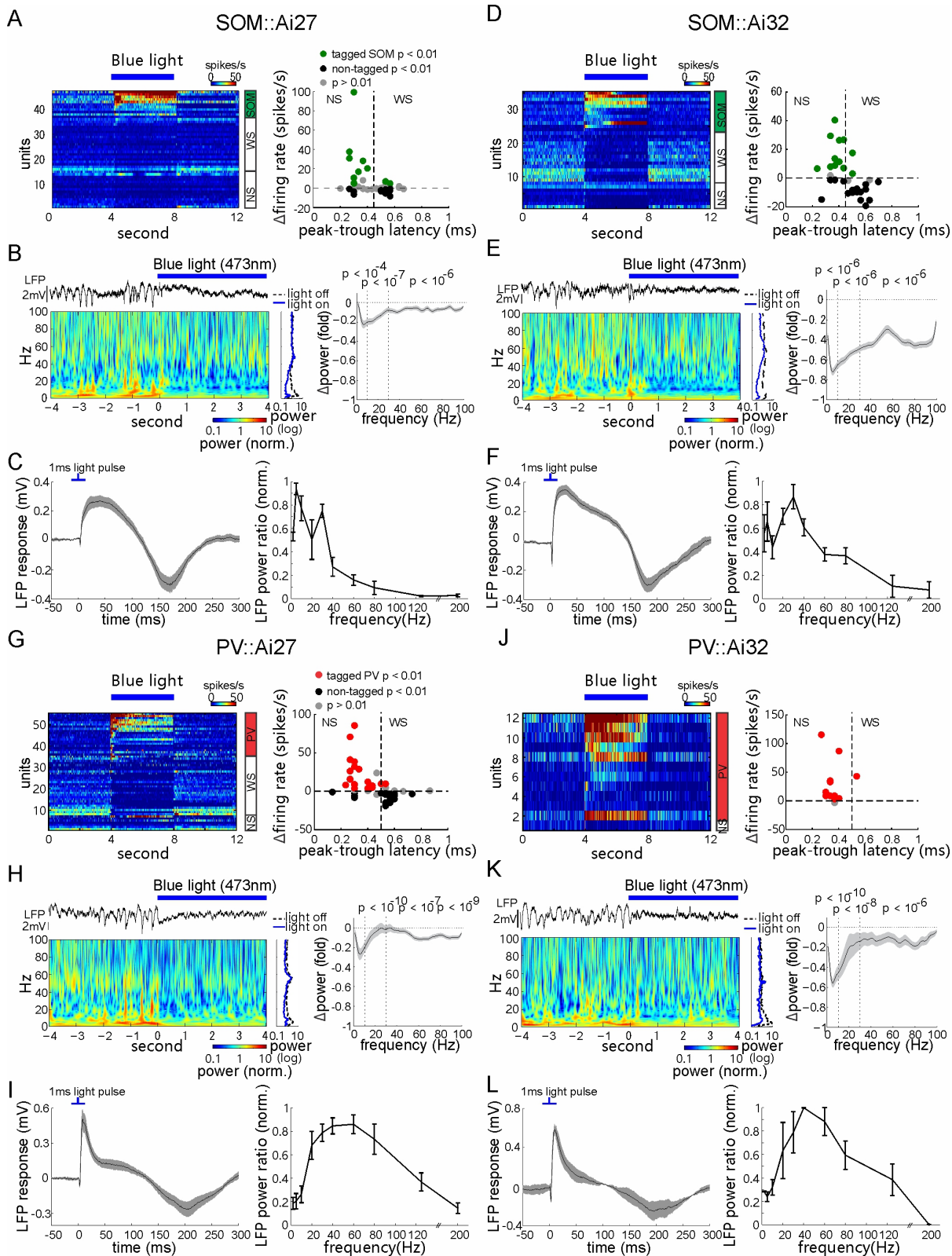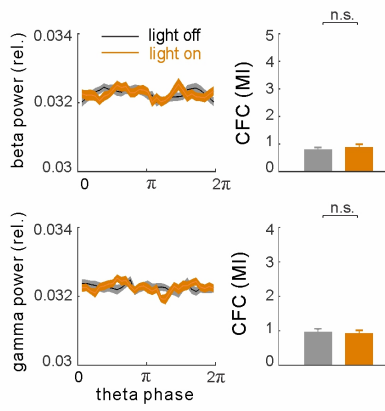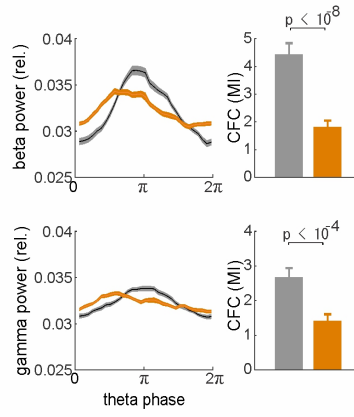
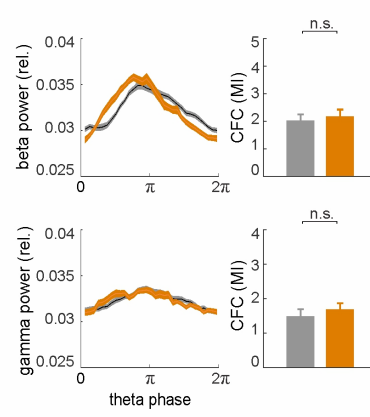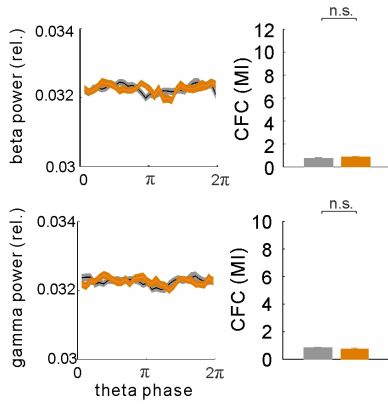**Figure S6 related to Figure 1, Figure 5 and Figure 7. Light induced spike rate and LFP responses in *SOM-ChR2* and *PV-ChR2* mice.** (A) Left: peri-stimulus time histograms (PSTHs) of spikes of recorded units, which were firstly sorted by the level of light induced firing rate changes and then classified as tagged SOM, non-tagged NS and BS groups. The spike rates were indicated by the color spectrum. Right: distribution of all units in the dimension of the peak-trough latency of spike waveforms and the light induced changes of firing rates (subtracted by the baseline level). Green: tagged SOM cells showing significant light induced increase of firing rate (n = 11 of 47 units in 8 *SOM::Ai27* mice, $p < 0.01$, permutation test). Black and gray: units showing significant firing rate decrease ($p < 0.01$, non-tagged) and non significant change ($p > 0.01$), respectively. (B) Left: an example trial of raw LFP segment (top) and the corresponding time-frequency spectrogram (bottom) before and during the laser light stimulation recorded in a *SOM::Ai27* mouse. Averaged power (over time) along with the frequencies during light off and light on period was shown (trial averaged, right inset). Right: summarized results of the light induced mean change of LFPs' power spectra (Δpower = [power$_{light\ on}$ − power$_{light\ off}$]/power$_{light\ off}$) from all recording in *SOM::Ai27* mice (n = 41 recording in 5 mice). Solid line is the mean value and shaded area represents s.e.m. *p* values of power changes in the delta/theta (1-10 Hz), beta (10-30 Hz) and gamma (40-80 Hz) bands were calculated by the *Wilcoxon* two-sided signed rank test. (C) Average LFP's response evoked by single light pulses (left, 9 recording in 4 mice) and light evoked LFP's power changes (power$_{light}$/power$_{baseline}$) of resonant activity at different stimulation frequencies (right, normalized to the maximum power change, error bar is s.e.m., n = 4 recording sites in 3 mice). (D-F) Similar to A-C except for *SOM::Ai32* mice. 12 of 35 units were tagged as SOM cells in 9 mice. For E, n = 32 recording in 12 mice. For average LFP response in F, n= 16 recording in 3 mice. For LFP power change in F, n= 5 recording in 3 mice. (G-I) Similar to A-C except for *PV::Ai27* mice. 19 of 55 units were tagged as PV cells in 20 mice. For H, n = 146 recording in 24 mice. For average LFP response in I, n= 10 recording in 7 mice. For LFP power change in I, n= 8 recording in 7 mice. (J-L) Similar to A-C except for *PV::Ai32* mice. 11 of 12 units were tagged as PV cells in 6 mice. For K, n = 75 recording in 8 mice. For average LFP response in L, n= 2 recording in 2 mice. For LFP power change in L, n= 2 recording in 2 mice.

SOM::Ai35

A

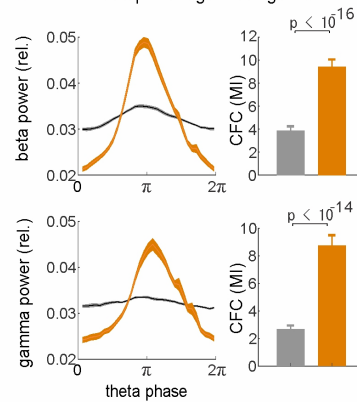B theta power: light on < light off

C theta power: light on > light off

PV::Ai35

D

E theta power: light on > light off

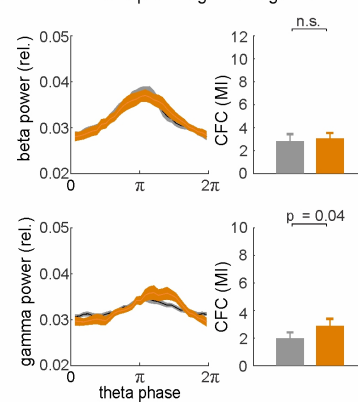F theta power: light on < light off

Figure S7 related to Figure 5. Correlation between light induced LFP CFC changes and LFP power changes.
(A) Cross-frequency phase-amplitude coupling (CFC) of theta-beta (top) and theta-gamma activity (bottom) of artificially generated random LFP signals which have same power spectra of the real LFP signals during light off (black) and light on (yellow) period in SOM::Ai35 mice. (B) CFC of theta-beta (top) and theta-gamma activity (bottom) of LFP trials showing light induced theta power decrease in SOM::Ai35 mice. (C) CFC of theta-beta (top) and theta-gamma activity (bottom) of LFP trials showing light induced theta power increase in SOM::Ai35 mice. (D-F) Similar to A-C except for recordings in PV::Ai35 mice. Solid line is the mean value and shaded area represents s.e.m. Error bars represent s.e.m. The *p* values were calculated by *Wilcoxon* two-sided signed rank test.